Chinese Chemical Letters 33 (2022) 3144–3150

Contents lists available at ScienceDirect

Chinese Chemical Letters

journal homepage: www.elsevier.com/locate/cclet

Bioelectronic modulation of single-wavelength localized surface plasmon resonance (LSPR) for the detection of electroactive biomolecules

Zetao Chen[a], Fenni Zhang[a], Yanli Lu[a], Yaru Li[a], Guang Liu[a], Jianzhen Shan[b], Qingjun Liu[a,*]

[a] Biosensor National Special Laboratory, Key Laboratory for Biomedical Engineering of Education Ministry, Department of Biomedical Engineering, Zhejiang University, Hangzhou 310027, China
[b] The First Affiliated Hospital, Zhejiang University School of Medicine, Hangzhou 310027, China

ARTICLE INFO

Article history:
Received 1 August 2021
Revised 3 October 2021
Accepted 12 October 2021
Available online 20 October 2021

Keywords:
LSPR
LED light
Bio-electron transfer
Electroactive biomolecule
Biosensor

ABSTRACT

The simplification of localized surface plasmon resonance (LSPR) detection can further promote the development of optical biosensing application in point-of-care testing. In this study, we proposed a simple light emitting diode (LED) based single-wavelength LSPR sensor modulated with bio-electron transfers for the detection of electroactive biomolecules. Indium tin oxide electrode loaded with nanocomposites of polyaniline coated gold nanorod was used as LSPR chip, and the applied electric potential was scanned at the LSPR chip for single-wavelength LSPR biosensing. Under the scanning of applied potentials, biological electron transfer of redox reaction was employed to demonstrate the bioelectronic modulation of single-wavelength LSPR for selective electroactive biomolecule detection. Without any additional recognition material, electroactive biomolecules uric acid and dopamine were detected directly with a sensitivity of 5.05 μmol/L and 7.11 μmol/L at their specific oxidation potentials, respectively. With the simplified optical configuration and selective bioelectronic modulation, the single-wavelength LSPR sensor is promising for the development of simple, low-cost, and high specificity optical biosensor for point-of-care testing of electroactive biomolecules.

Localized surface plasmon resonance (LSPR) is a nanoscale phenomenon that absorbs photon energies of incident light at the resonant frequency of noble metal nanostructures, which is ultrasensitive to surrounding refractive index changes for label-free, reliable, and real-time biochemical detections [1,2]. Thus, LSPR has been widely used in the detection of biomolecules, such as protein, DNA molecules, fat, glycan [3–7]. Most of the traditional LSPR systems are based on the detection of optical spectrum, which necessitate complicated space-consuming light source, making it difficult for practical applications [1]. Therefore, a simple and miniaturized LSPR system is needed for the development of portable, affordable, and highly sensitive biosensor for point-of-care applications.

Single-wavelength LSPR is often used for miniaturized LSPR detection, which simply monitors the optical extinction at a single-wavelength [8]. This method has relatively low requirements on the light source, and even a simple light-emitting diode (LED) can be used for LSPR detection. To construct a more accurate single-wavelength LSPR, the potential-scanning LSPR (p-LSPR) was proposed to measure the local refractive index change with potential scan instead of wavelength scan, as the optical extinction of the nanoparticle are sensitive to external potentials [9–11]. By depositing noble metal nanoparticles onto the indium tin oxide (ITO)-based transparent glass substrate, the LSPR chip can be fabricated for both electric potential stimulation and optical extinction detection. Combined with a single-wavelength light source such as LED, p-LSPR can be used for the construction of single-wavelength LSPR sensor with a simplified configuration. With further integration of a miniaturized and easy-to-implement potential control circuit [12–14], the single-wavelength LSPR with scanning potentials is promising for portable biosensing applications.

Biological electron transfers exist in almost all of the life activities, such as cell metabolism and signal transduction [15,16]. During these activities, electroactive biomolecules are significant electron transfer carriers [17]. Therefore, the detection of electroactive biomolecules can help evaluating the metabolic levels and monitoring the status of life activities. For example, the detection of some electroactive biomolecules such as uric acid in urine can

* Corresponding author.
E-mail address: qjliu@zju.edu.cn (Q. Liu).

https://doi.org/10.1016/j.cclet.2021.10.027
1001-8417/

evaluate the risk of gout, and the detection of electroactive neurotransmitters such as dopamine and histamine can help predicting the neurological diseases [18–20]. In LSPR sensing, the resonant wavelength of LSPR nanoparticle is dependent on the surface electron density [21], thus the biological transferred electrons can be employed to modulate the optical extinction for electroactive biomolecule detection. With the applied potentials, redox reaction of the electroactive biomolecules will be initiated and the corresponding electron transfer will occur, which peaks at the specific redox potential [22,23], resulting in the maximum electron modulation. Besides, as different electroactive biomolecules have different oxidation potentials [24], the biological electron transfer modulated LSPR will enable the specificity of the single-wavelength LSPR sensor for electroactive biomolecule detection without any additional recognition materials.

In this paper, we proposed a LED-based single-wavelength LSPR sensor for the detection of electroactive biomolecules based on the biological electron transfer modulation of LSPR. Nanocomposites of gold nanorods coated with polyaniline were fabricated for the enhancement of electrical sensitivity. By loading the nanocomposites onto ITO electrode, the LSPR chip was fabricated for both potential scan and optical detection. Combined with LED illuminating, a single-wavelength LSPR sensor with scanning potentials was constructed for simple and low-cost LSPR measurement. The electrical properties of this single-wavelength LSPR sensor were firstly characterized with both the finite-difference time-domain (FDTD) simulation and the recorded potential-extinction spectrum over the applied potentials. Then, to demonstrate the bioelectronic modulation of the LSPR, electron transfers during the redox of specific electroactive biomolecules were evaluated. Finally, based on this specific electron transfer properties of the electroactive biomolecules, dopamine and uric acid were detected to evaluate the capability of this LED-based single-wavelength LSPR sensor.

LSPR chips were prepared for the detection of optical extinction and the applying of electric potentials. Through physical vapor deposition (PVD), a layer of thin ITO film was deposited on a transparent glass substrate in form of three electrodes to construct a transparent electrochemical three electrode system with electrode lead on one end, namely ITO chip. Then the ITO chips were immersed in polyetherimide (PEI) solution (10 mg/mL) for 30 min to cover their surface with a thin layer of adhesive PEI for the immobilization of nanocomposites. To boost the testing stability of the electrodes, after the ITO layer is deposited, silver/silver chloride paste and carbon paste were screen-printed to reference electrode and counter electrode position of the ITO chips, respectively. The prepared polyaniline (PANI) coated gold nanorods (AuNRs) nanocomposites (AuNRs@PANI) was centrifuged at 12,000 rpm for 15 min and the precipitate was re-dispersed with 0.35 mL ultrapure water (The reagents and apparatus and the synthesis of plasmonic nanocomposites were deposited in Supporting information). Afterwards, the nanocomposites were immobilized to the PEI modified working electrode surface by spray casting the aqueous dispersion as functional modification. The spray distance was set at 6 cm and the spray pressure was set at 18 psi. Afterwards, the modified ITO chips were immersed in ultrapure water for 12 h to remove the excess sodium dodecyl sulfate (SDS) and were subsequently immersed in 0.2 mol/L HCl solution for 1 h to dope the coated PANI with H^+. The nanocomposites immobilized ITO chips that can perform optical detection and electrochemical simulation simultaneously were then used as LSPR chip.

Theoretical calculations of finite-difference time-domain (FDTD) on LSPR of the nanostructures were performed for the simulation and explanation of plasmonic potential sensitivity. Single AuNR was modeled in aqueous medium and on ITO substrates with hexadecyl trimethyl ammonium bromide (CTAB) coating and either PANI shells. Refractive index values for ITO, gold, PANI and water were obtained from the included materials database. Dimensions for the AuNRs and the PANI coating thicknesses for simulations were obtained from TEM measurements. All simulations were performed with a 0.2 nm mesh size in the x, y and z directions. The simulation region boundaries of x and y directions were set as periodic, and z direction was set as perfectly matched layer (PML). Plane wave light source ranged from 300 nm to 880 nm with an electric field amplitude of 1 V/m was applied for the stimulation of plasmonic models. To obtain the electromagnetic field distribution of the plasmonic nanoparticles, the frequency-domain field and power monitor was set across the center of nanostructures and parallel with ITO substrate.

Based on the LSPR chip, electrochemical coupling LSPR experiments were conducted for the sensitivity exploration of electric potentials to optical extinction and the construction of single-wavelength LSPR sensor. LSPR chip was inserted into quartz cuvette with its electrode lead connected to electric potential controller. The incident light with a wavelength range of 300–880 nm was illuminated on the back of LSPR chips. The transmitted light was detected by a spectrophotometer with 0.38 nm optical path. Electrochemical workstation was treated as electric potential controller, and electric potentials ranged from −0.4 V to 0.6 V with an interval of 0.1 V were applied to the LSPR chips under the solvent of 0.01 mol/L PBS with adjusted pH of 7.2. The corresponding optical extinctions were recorded for the study of electric potential modulation of LSPR. Afterwards, the relationship of applied potential and the optical extinction at certain wavelength of incident light was analyzed for the study of single-wavelength LSPR detection.

To investigate the bioelectronic modulation of plasmonic extinction under the scanning potentials, the electrochemical redox reaction of electroactive biomolecule uric acid was analyzed as a demonstration. A step potential was used as the scanning potentials. Under the scanning potentials from −0.4 V to 0.6 V with an interval of 0.1 V, the PBS solution of uric acid with a concentration of 100 μmol/L was added into a quartz cuvette. This cuvette was used as electrochemical cell at the same time. Under the scanning potentials, the electric current changes of LSPR chips were collected for the electron transfer analysis. By recording the optical extinction spectrum of uric acid and bare PBS at different applied potential, the bioelectronic modulation of LSPR was analyzed for single-wavelength measurement.

Based on the LSPR chips, single-wavelength LSPR sensor was constructed for the detection of electroactive biomolecules. Using single-wavelength LED as incident light source, the transmitted light was captured by an optical fiber. While potentials ranged from 0 V to 0.6 V with an interval of 0.001 V were applied on LSPR chips, electroactive biomolecule uric acid with concentrations of 20, 40, 60, 80 and 100 μmol/L were detected. For the analysis of sensing specificity, electroactive biomolecule dopamine solutions (in 0.01 mol/L PBS) with concentrations ranged from 20 μmol/L to 100 μmol/L were also tested under the same condition.

The traditional LSPR sensor measures the optical extinction of the noble metal nanostructure with wavelength scan for local refractive index change detection. This spectrum-based detection requires complex light source, which is space consuming and costly. As the optical extinction of the LSPR nanoparticle is sensitive to applied potentials, the simple single-wavelength LSPR can be constructed with applied potential scan instead of wavelength scan, namely p-LSPR. The p-LSPR is sensitive to both refractive index and surface charge density, and can be modulated by the biological electro transfer. Besides, the resolution of p-LSPR is mainly based on the interval of scanning potentials, which could be easily decreased to sub-microvolt (10^{-6} V) and is more accurate than optical path-based traditional LSPR detection. Due to the low

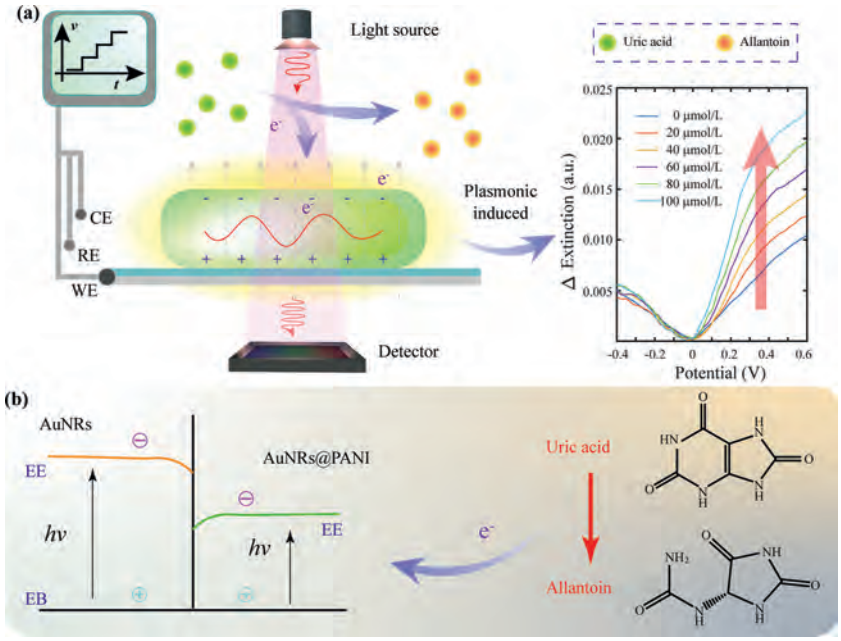

Fig. 1. Schematic diagram of the LED-based single-wavelength LSPR for the detection of electroactive biomolecules. (a) Using LED as light source, while the scanning potentials were applied to the LSPR chip, extinction changes along with the applied potentials were recorded for the detection of electroactive biomolecule such as uric acid. (b) With the coating of PANI, the decreased band gap of nanocomposite improved the sensitivity of optical extinction to electrical stimulates.

requirement for light source, even a simple LED can be used for the p-LSPR detection, which is space saving and low cost.

Fig. 1a shows the schematic diagram of electron transfer modulated single-wavelength LSPR for electroactive biomolecules detection. A single-wavelength LED was used as the incident light source. AuNRs with controllable aspect ratio were synthesized for the generation of LSPR. By depositing the nanocomposites of PANI coated AuNRs on the ITO electrode, the LSPR chip was fabricated for both potential scan and optical detection. The light of LED illuminated on the nanocomposites stimulates the LSPR effects and the transmitted light was recorded by a portable spectrum detector. Due to the sensitivity of optical extinction to applied potentials, a potential-extinction spectrum was formed based on the detection of extinction intensity for the sensing of electroactive biomolecules.

The nanocomposites of AuNRs@PANI were formed with PANI coating for a decreased band gap to further improve the sensitivity of electrical stimulations (Fig. 1b). Under the positive scanning of applied potentials, electroactive biomolecules such as uric acid was oxidized into allantoin and electrons were transferred to the nanocomposites for the bioelectronic modulation of the optical extinction of LSPR. The changes of extinction along with electric potential illustrated the number of electrons transferred. At the oxidation potential point, there comes a maximum optical extinction change, which was recognized as feature of the sensor specificity. Since different electroactive biomolecules have different oxidation potentials, the oxidation potentials were used for the distinction of different electroactive biomolecules.

LSPR chips are consisted of AuNRs based nanocomposites and ITO electrodes. The AuNRs were synthesized for the optical plasmonic extinction detection based on seeded growth method, in which the volume of $AgNO_3$ controls the aspect ratio of AuNRs (Table S1 in Supporting information). The one with 0.2 mL $AgNO_3$ showed optimal interval between extinction peaks, and reasonable extinction peak intensity ratio was selected for the following experiments (Fig. S1 in Supporting information). Based on the morphological characterization (Fig. S2a in Supporting information), the average length of the used AuNRs was about 50 nm and the average transverse diameter was about 20 nm. Furthermore, nanocomposite of AuNRs@PANI was synthesized through oxidative polymerization for p-LSPR sensing with improved sensitivity to electrical potential (Fig. 2a). After the polymerization, the nanocomposites were synthesized and exhibited a complex waveform with two peaks and a shoulder (Fig. 2b). The peak at about 550 nm represents the transverse feature of AuNRs, the peak at about 810 nm represents the PANI coating, and the wave shoulder at about 700 nm represents the mix of longitudinal feature of AuNRs and the PANI coating. Compared to the optical extinction of bare gold nanorods (the blue curve), the transverse peak of the nanocomposites had a small red shift because of the PANI coatings. Compared to the optical extinction of bare PANI (the red curve), the longitudinal peak of the nanocomposites was almost the same. Besides, the coating layer of the nanocomposites can be observed around the AuNRs from the TEM images (inset of Fig. 2b and Fig. S2b in Supporting information).

ITO electrode was fabricated as substrate for electric potential application. By PVD, a thin layer of ITO film was deposited on the transparent glass (Fig. 2a). Through the spray casting of nanocomposites onto the ITO surface, LSPR chips was constructed for the potential stimulation and extinction detection simultaneously. Compared with bare AuNRs loaded ITO electrode (Fig. S2c in Supporting information), the nanocomposites loaded ITO electrode are thicker (inset of Fig. 2c and Fig. S2d in Supporting information), which means the nanocomposites were successively immobilized on the ITO surface. After doping in proton acid, the nanocomposites exhibit obvious extinction peaks illustrating a more recognizable signal (Fig. 2c).

To characterize the properties of the fabricated LSPR chip, optical and electrochemical methods were employed. The optical tests for a single chip showed high repeatability in extinction detection (Fig. S3a in Supporting information), and the results of different chips showed reasonable repeatability (Fig. S3b in Supporting information). Electrochemical cyclic voltammetry (CV) peaks of the nanocomposites loaded chips are higher than bared chips indicating the improvement of electrochemical properties after the loading of nanocomposites (Fig. 2d). Meanwhile, separate CV tests for

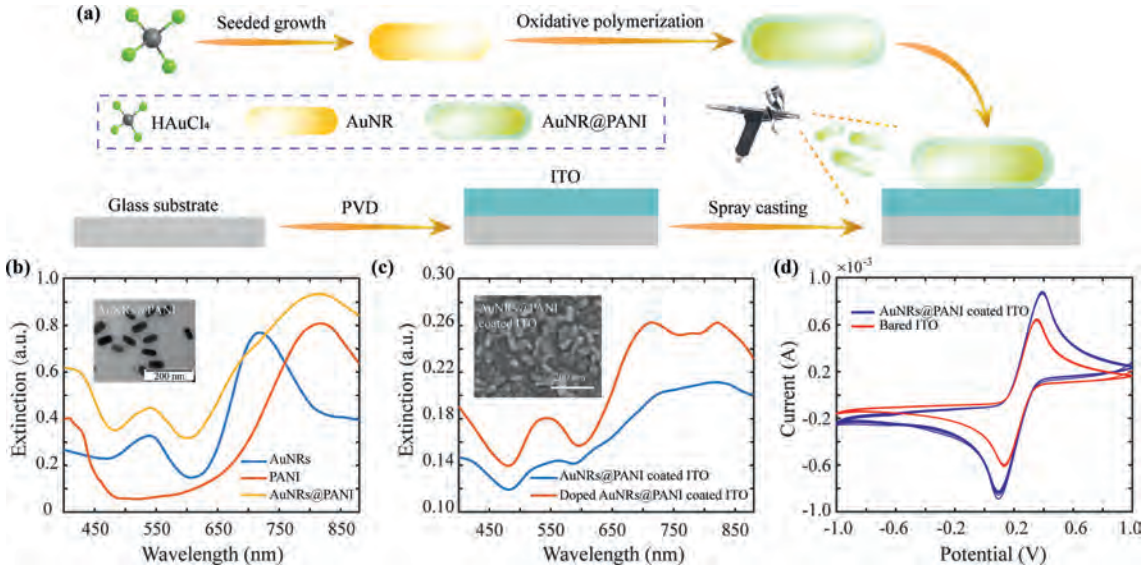

Fig. 2. Construction of LSPR chips. (a) The synthesis of AuNRs@PANI nanocomposites through seeded growth and oxidative polymerization, and the fabrication of LSPR chips through PVD and spray casting. (b) Optical extinction comparison of AuNRs, PANI, and AuNRs@PANI (The inset is TEM image of AuNRs@PANI.). (c) Optical extinction comparison of AuNRs@PANI coated ITO, and its proton doped mode (The inset is SEM image of the chip surface.). (d) Cyclic voltammetry (CV) sweeping of bare ITO chips and the nanocomposites loaded ITO chips for 5 times respectively showing the coating enhancement of electrochemical properties and the good electrochemical stability of the LSPR chips.

nanocomposites coated ITO chips and bare ITO both showed good repeatability for p-LSPR measurement. Furthermore, the potential sensitivity of AuNRs was compared with gold nanospheres (diameter of 50 nm) (Fig. S4 in Supporting information). The slope of longitudinal AuNRs mode is greater than the nanospheres, while the transverse AuNRs mode is smaller than the nanospheres. Therefore, the longitudinal mode of AuNRs was used for high sensitivity detection.

Through the polymerizing of PANI on AuNRs, band gap of the nanocomposite was decreased compared to bare AuNRs [25,26]. By loading the nanocomposites on ITO substrate, the photoelectrical and the electrical sensitivity were improved. Also, with the PANI coating, the resistance of the working electrode of the LSPR chip was reduced leading to an easier electron transfers on the surface of nanocomposites [27–29]. Therefore, the LSPR sensitivity of the nanocomposites to applied potentials or surrounding electromagnetic field were enhanced. On the other hand, the coating of PANI increased the interval between AuNRs and eliminated the aggregation during the scanning of applied potentials, which help improve the stability of the LSPR chip and the single-wavelength LSPR detection [30]. Besides, the influence factors on the potential sensitivity of LSPR include solution pH, surrounding temperature, and electromagnetic interference, *etc*. For example, the changes of pH affect the doping mode of the PANI coatings. When the solution pH is increased, the plasmonic peaks responded a red-shift (Fig. S5 in Supporting information). To avoid the interference caused by these factors, all the experimental conditions except for variables were set identical.

To explore the potential modulation on optical extinction in our LSPR sensor, the electromagnetic field (EF) distribution was calculated through FDTD. The 3-dimentional structure of nanocomposite (Fig. S6a in Supporting information) and bare AuNR (Fig. S6b in Supporting information) were illuminated under plane light source, and the EF was observed strong at the two tips of the AuNR (Fig. 3a) and nanocomposite (Fig. 3b), which means the longitudinal mode of AuNRs is more sensitive in plasmonic resonance. Compared to the EF of AuNR, a more uniform EF distribution was observed of nanocomposite with smaller EF intensity, which means the nanocomposites is more sensitive to surrounding electron transfers after the coating of PANI. Since paired nanocomposites could be seen on the LSPR chips, EF of AuNRs@PANI dipole was also calculated with same settings. Compared with the calculated EF of single nanocomposite, the average intensity of the dipole's excitation EF at longitudinal mode is slightly decreased (Fig. 3c). However, the minimum changes of plasmonic resonance imply the impact of paired situation for assembled nanocomposites modified chip was negligible.

Based on the simulation, the optical extinction responses with applied electric potentials were detected for the evaluation of single-wavelength LSPR sensor. With the applied electric potentials, obvious extinction intensity changes in both transverse and longitudinal peaks of AuNRs (Fig. 3d) and nanocomposites (Fig. 3e) were observed. Due to the reduced damping of PANI coating, the optical extinction changes of the nanocomposites loaded chips was more sensitive to applied potentials compared to the bare AuNRs based LSPR chips at longitudinal mode (Fig. 3f). Also, at transverse mode, the optical extinction changes of nanocomposites coated LSPR chips were enhanced compared to that of bare AuNRs coated LSPR chips (Fig. S7 in Supporting information), but the enhancement was weaker than longitudinal mode.

Charge density of the nanocomposites can be controlled by applied potentials, and the effects of charge densities can be observed with optical extinction intensity changes or peak shifts in the optical spectrum [10,31,32]. Therefore, with the simulation of electric potentials, the charge density of nanocomposites will change and the stimulation effects can be monitored by optical extinction. For the traditional wavelength-scanning LSPR detection, the detection results were mainly depended on the extinction peak wavelength shift [9]. Limited by the optical path of grating in spectrometer, the recognized wavelength shift was about subnanometer according to the manufacturing process of gratings. For the detection of optical extinction intensity, the resolution could be greatly improved by using high-precision analog-to-digital conversion chip, which is easier to realize than optical path update.

Biochemical reactions of electrochemical redox usually involve the bio-electron transfers. Under the scanning potentials, the electroactive uric acid underwent redox reaction and the optical extinction intensity changed with applied potentials. Along with the

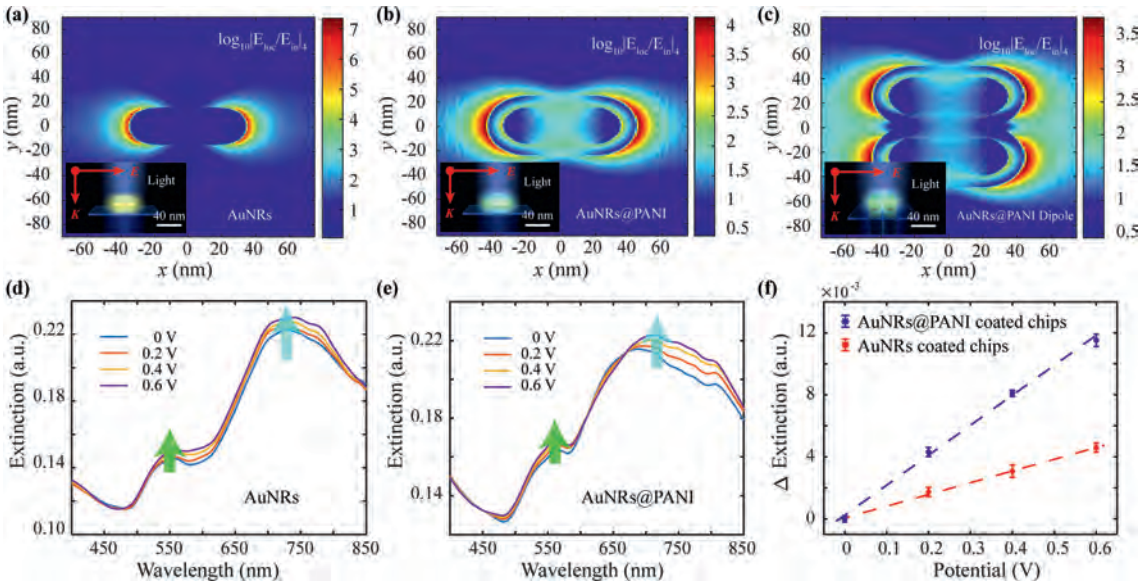

Fig. 3. Electromagnetic field (EF) distributions of nanostructures and their electric potential modulation. (a) EF distribution of bare AuNRs at longitudinal mode (The inset is the scheme of bare AuNRs structure.). (b) EF distribution of the AuNRs@PANI at longitudinal mode (The inset is scheme of the AuNRs@PANI structure.). (c) EF distribution of the paired AuNRs@PANI at longitudinal mode (inset is scheme of paired AuNRs@PANI structure). (d) Electric potential modulation of AuNRs' optical extinction. (e) Electric potential modulation of AuNRs@PANI's optical extinction. (f) The extinction response of AuNRs@PANI coated LSPR chips and AuNRs coated LSPR chips at longitudinal mode.

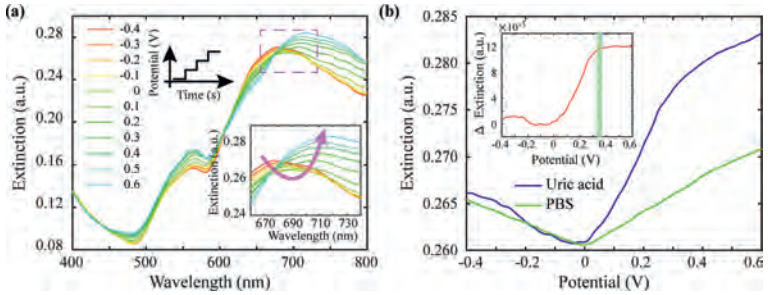

Fig. 4. Modulation of biochemical reaction electron transfer to LSPR. (a) The transferred electrons generated by uric acid' oxidation affect the optical spectrum along with the applied potentials. (b) At 710 nm, the extinction intensity of uric acid and PBS along with applied potentials (The inset shows the extinction difference of uric acid and PBS, the inflection point of the rising appears at about 0.35 V.).

scanning potentials, the optical extinction spectra at different electric potentials were showed in Fig. 4a. At about 710 nm, the intensity changes of longitudinal peak relatively greater (inset of Fig. 4a). Therefore, the intensities at wavelength of 710 nm for each applied potential were extracted, and then the potential-extinction spectrum was formed for single-wavelength biosensing (Fig. 4b). Compared with the potential-extinction curve of PBS solution (green curve in Fig. 4b), the potential-extinction curve of uric acid showed obvious shift (blue curve in Fig. 4b). By subtracting the reference spectrum of PBS, the potential-extinction spectrum of uric acid was obtained, and the maximum extinction changes was at applied potentials of about 0.35 V (inset of Fig. 4b). As the oxidation potential of uric acid is also 0.35 V, this maximum extinction response potential of potential-extinction spectrum could be recognized as sensing specificity.

Based on the layered structure of LSPR chip, for better understanding of the single-wavelength LSPR and for the calculation of electron transfer rate, the LSPR chip was equivalent to an impedance electrical circuit model, which is composed of interlayer capacitors and layer resistors as function of $Z = f(C, R)$ (Fig. S8 in Supporting information). This equivalent electrical circuit describes the electrochemical interactions between the nanocomposites and the conducting surface. The charge transfer resistance (R_{ct}) was calculated through model fittings based on the solution resistance, nanocomposite capacitance and resistance, and other modeling elements. Based on this equivalent electrical circuit, number of transferred electrons, electron density, and the volume of reactant was calculated through model fitting (Fig. S9 in Supporting information). Based on the definition of electric charge quantity Q, the charge transfer rate was analyzed with the optical extinctions (Fig. S10 in Supporting information). For example, the plasmonic extinction changes of 100 μmol/L uric acid solution was about 0.0117 (a.u.), and the number of transferred electrons was calculated according to $Q = It = ne$, namely 3.62 × 1013 electrons were transferred per second. Here, I is the detected electric current, t is time, n is the amount of electrons, and e is the elementary charge constant.

In electrochemical redox reactions, there are electron exchanges between electrode and reactants [33]. In general, the reactant was acted as electron donor and the working electrode was acted as electron acceptor in oxidation reaction. Under positive scanning of electric potentials, uric acid was oxidized into allantoin. During this oxidized process, ring of the uric acid was untied and two electrons were lost for each uric acid molecule [34]. Under the driving of applied potentials, electrons generated from the oxidation reaction were transferred to the nanocomposites on LSPR chip. Then the distribution of electron density of the nanocomposites was affected and the optical extinction intensity was changed. Through the detection of potential-extinction spectrum, single-wavelength optical biosensing was realized. For different electroac-

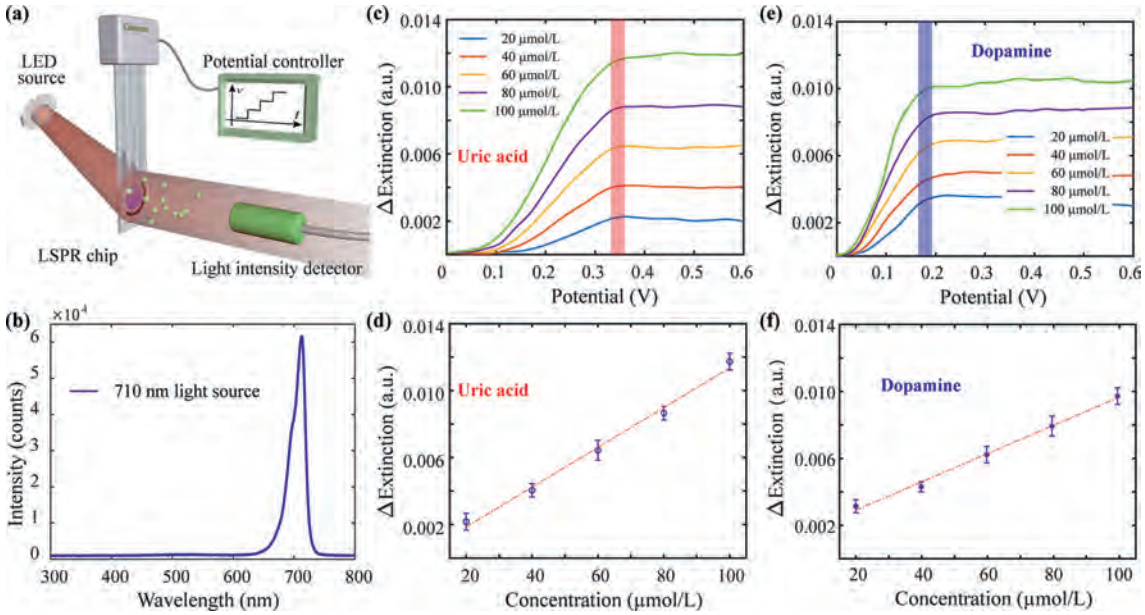

Fig. 5. The detection of electroactive biomolecules of uric acid and dopamine. (a) Schematic diagram of the single-wavelength optical detection of electroactive biomolecules. (b) The optical characterization of 710 nm single-wavelength LED. (c) The extinction changes for different concentrations of uric acid. (d) At 0.35 V, the extinction changes of uric acid increase along with concentrations. (e) The extinction changes for different concentrations of dopamine. (f) At 0.18 V, the extinction changes of dopamine increase along with concentrations.

tive biomolecules, their oxidation potentials were generally different. At the oxidation potential of electroactive biomolecules, there will be a prominent response of electron transfers on the potential-extinction spectrum. Therefore, the specificity for the single-wavelength LSPR detection of electroactive biomolecules could be determined by their oxidation potentials.

To demonstrate the capability of single-wavelength LSPR, electroactive biomolecule of uric acid with different concentrations was detected. With the illuminating of single-wavelength LED, the extinction intensity changes were detected with applied scanning potentials (Fig. 5a). The optical characterization of the LED showed a narrow tip on 710 nm indicating the good monochromaticity of the light source (Fig. 5b). The working status of the LED was tested as 0.6 A of working current and 2.62 V of working voltage. By adding the uric acid solution with different concentrations, the electrons generated by the electrochemical oxidation were transferred to the LSPR chip. The oxidation currents were recorded, and the oxidation potential is at 0.35 V (Fig. S11a in Supporting information). Stimulated to the LSPR chips, the optical extinction increased correspondingly (Fig. S11b in Supporting information). With baseline subtraction, potential-extinction spectrum of nanocomposites corresponding to each uric acid concentration at 710 nm were obtained (Fig. 5c), and the differential extinction increased linearly over the uric acid concentrations (Fig. 5d). Thus, based on this single-wavelength LSPR sensor, the electroactive biomolecule uric acid was detected. The limit of detection was calculated to be 5.05 μmol/L.

To further evaluate the specificity of this single-wavelength LSPR sensor, electroactive biomolecule dopamine was also detected. As the dopamine solution (in 0.01 mol/L PBS) was added into the cuvette, electrons generated from the electrochemical oxidation of dopamine were transferred to the LSPR chip. The corresponding current detected for comparison of the electrochemical signals and optical signals (Fig. S11c in Supporting information). The oxidation peak of dopamine was at 0.18 V. Stimulated on the LSPR chip, the optical extinction changes were recorded correspondingly (Fig. S11d in Supporting information). With baseline subtraction, potential-extinction spectrum of nanocomposites corresponding to each dopamine concentration at 710 nm were obtained (Fig. 5e), and the differential extinction increased linearly over the dopamine concentrations (Fig. 5f). Therefore, the electroactive biomolecule dopamine was detected based on this single-wavelength LSPR sensor and the limit of detection was calculated to be 7.11 μmol/L.

Strategies for the detection of electroactive biomolecules include both electrochemical and optical methods. Under the stimulation of electric potentials, redox reaction could easily occur. Thus, the electrochemical approaches, including differential pulse voltammetry (DPV), square wave voltammetry (SWV) and cyclic voltammetry (CV) are usually utilized for the fast and reliable detection of electroactive biomolecules (Table S2 in Supporting information). Although the electrochemical approaches with different nanomaterials or technologies were effective for the detection of electroactive molecule, the optical strategies showed advantages [35,36]. Nanomaterials based fluorescence methods with improved sensitivity were utilized for the detection of uric acid or dopamine due to their redox properties (Table S2). However, during these detections, oxidases for the specific promotion of molecules oxidation were usually needed making the sensing limited by surrounding conditions. Even for non-enzyme detections, complex set or nanocomposites were often needed for the improvement in sensitivity. What's more, several considerations regarding the materials, architectures and fabrication methods used need to be carefully evaluated to advance this field. With similar detection ranges and lower detection limits, LSPR can provide richer spatial information. In our study, single-wavelength LSPR combined electrochemical and optical realized non-enzyme free label detection of electroactive biomolecules.

This single-wavelength LSPR platform is realized by the mechanism of electron transfer modulation of plasmonic resonance, which is of great significance in the development of miniaturization and portability of optical sensing with the single-wavelength extinction extraction and easy-to-implement potential control. Compared with electrochemical methods, this single-wavelength LSPR is advanced in sensitivity and anti-electromagnetic interference performance. Compared with traditional LSPR, this single-

wavelength LSPR does not require extra space and device for wavelength scanning, making it a valuable platform for miniaturization and cost reduction. Based on the single-wavelength LSPR platform, the mechanism of bioreaction's electron transfer modulation on optical extinction was studied and utilized for sensing applications, which is significant in the field of bioelectronics. Furthermore, there has been great interest in the single-wavelength LSPR sensing as a fast, simple, low-cost medical diagnostic technology, which can be widely used in several biomedical areas including molecular dynamics research, point-of-care diagnostics, and drug discovery.

In summary, we have investigated the significant influence of bio-electrons transfer in LSPR and proposed a LED-based single-wavelength LSPR sensor for the detection of electroactive biomolecules. With the coating of PANI, the electric sensitivity of nanocomposites on optical extinction was enhanced. With the sensitive influences of electron transfers to plasmonic resonance, electroactive biomolecules of uric acid and dopamine were detected as demonstrations for analyzing the modulation of electroactive biomolecules' electrochemical process to LSPR. With the simplified optical configuration and the easy-to-implement electric control, this single-wavelength LSPR sensor is promising for miniaturized measurement and label free detection of biomolecules, which is valuable for practical applications in point-of-care settings.

Declaration of competing interest

The authors declared that they had no conflict of interest.

Acknowledgments

This work was supported by the National Natural Science Foundation of China (Nos. 81971703, 81801793, 31671007), the China Postdoctoral Science Foundation (Nos. 2018M630677, 2019T120518), the National Key Research and Development Program (No. 2018YFC1707701), the Zhejiang Provincial Natural Science Foundation of China (No. LZ18C100001), the Fundamental Research Funds for the Central Universities (Nos. 2021QNA5018, 2021FZZX002-05) and the Collaborative Innovation Center of Traditional Chinese Medicine Health Management of Fujian Province of China.

Supplementary materials

Supplementary material associated with this article can be found, in the online version, at doi:10.1016/j.cclet.2021.10.027.

References

[1] K.M. Mayer, J.H. Hafner, Chem. Rev. 111 (2011) 3828–3857.
[2] J.R. Mejía-Salazar, O.N. Oliveira, Chem. Rev. 118 (2018) 10617–10625.
[3] H.M. Kim, J.H. Park, D.H. Jeong, H.Y. Lee, S.K. Lee, Sens. Actuat. B: Chem 273 (2018) 891–898.
[4] M. Lu, M. Lin, F. Wang, Y. Zhang, W. Peng, Nanomaterials 11 (2021) 1–10.
[5] A. Gowri, A.S. Rajamani, B. Ramakrishna, V.V.R. Sai, Opt. Fiber Technol. 47 (2019) 15–20.
[6] J. Yang, A. Moraillon, A. Siriwardena, et al., Anal. Chem. 87 (2015) 3721–3728.
[7] B. Sepúlveda, P.C. Angelomé, L.M. Lechuga, L.M. Liz-Marzán, Nano Today 4 (2009) 244–251.
[8] J.W. Lee, G. Ha, J. Park, et al., ACS Appl. Mater. Interfaces 12 (2020) 36339–36346.
[9] H. Nishi, S. Hiroya, T. Tatsuma, ACS Nano 9 (2015) 6214–6221.
[10] L. Ran, Y. Tao, K. Guo, et al., Phys. Chem. Chem. Phys. 20 (2018) 2146–2150.
[11] T. Okazaki, T. Orii, S.Y. Tan, et al., Anal. Lett. (2021) 1951749.
[12] D. Ji, N. Xu, Z. Liu, et al., Biosens. Bioelectron. 129 (2019) 216–223.
[13] S.S. Low, Y. Pan, D. Ji, et al., Sens. Actuat. B: Chem. 308 (2020) 127718.
[14] G. Xu, C. Cheng, Z. Liu, et al., Adv. Mater. Technol. 4 (2019) 1–13.
[15] M.B. Bhavsar, L. Leppik, K.M. Costa Oliveira, J.H. Barker, Front. Bioeng. Biotechnol. 8 (2020) 603.
[16] M.M. Kaelberer, K.L. Buchanan, M.E. Klein, et al., Science 361 (2018) eaat5236.
[17] C. Angione, Biomed. Res. Int. 2019 (2019) 8304260.
[18] N. Dalbeth, H.K. Choi, L.A.B. Joosten, et al., Nat. Rev. Dis. Prim. 5 (2019) 69.
[19] P.D. Morrison, R.M. Murray, Ther. Adv. Psychopharmacol. 8 (2018) 127–135.
[20] S.E. Hyman, Curr. Biol. 15 (2005) R154–R158.
[21] J.A. Jackman, A. Rahim Ferhan, N.J. Cho, Chem. Soc. Rev. 46 (2017) 3615–3660.
[22] A. Radoi, D. Compagnone, Bioelectrochemistry. 76 (2009) 126–134.
[23] K. Asami, H. Nishi, T. Tatsuma, Nanoscale. 8 (2016) 14092–14096.
[24] K. Wątor, D. Dobrzyński, K. Sugimori, E. Kmiecik, Int. J. Biometeorol. 64 (2020) 815–826.
[25] J.W. Jeon, J. Zhou, J.A. Geldmeier, et al., Chem. Mater. 28 (2016) 7551–7563.
[26] N. Jiang, L. Shao, J. Wang, Adv. Mater. 26 (2014) 3282–3289.
[27] A. Ray, G.E. Asturias, D.L. Kershner, et al., Synth. Met. 29 (1989) 141–150.
[28] G. Liao, Q. Li, Z. Xu, Prog. Org. Coat. 126 (2019) 35–43.
[29] S. Zhang, C. Ran, S. Chen, et al., J. Electrochem. Soc. 164 (2017) 1021–1027.
[30] J.W. Jeon, P.A. Ledin, J.A. Geldmeier, et al., Chem. Mater. 28 (2016) 2868–2881.
[31] X.Y. Zhang, D. Han, N. Ma, et al., J. Phys. Chem. Lett. 9 (2018) 6047–6051.
[32] B.S. Hoener, H. Zhang, T.S. Heiderscheit, J. Phys. Chem. Lett. 8 (2017) 2681–2688.
[33] H. Gerischer, J. Phys. Chem. 95 (1991) 1356–1359.
[34] A. Andries, S. De Rechter, P. Janssens, D. Mekahli, A. Van Schepdael, J. Chromatogr. B. 1096 (2018) 201–207.
[35] P.A. Rasheed, J.S. Lee, Microchim. Acta 184 (2017) 1239–1266.
[36] Q. Wang, X. Wen, J. Kong, Crit. Rev. Anal. Chem. 50 (2020) 359–375.